Experimental and theoretical study of the strong dependence of the microstructural properties of $Sr_xBa_{1-x}Nb_2O_6$ thin films as a function of their composition

P. R. Willmott,[1,*] R. Herger,[1] B. D. Patterson,[1] and R. Windiks[2]
[1]*Swiss Light Source, Paul Scherrer Institute, CH-5232 Villigen, Switzerland*
[2]*Condensed Matter Theory Group, Paul Scherrer Institute, CH-5232 Villigen, Switzerland*
(Received 17 November 2004; published 29 April 2005)

We report an experimental and theoretical study of the strong dependence of the crystalline texture of thin films of $Sr_xBa_{1-x}Nb_2O_6$ grown on MgO(001) on the Sr-content x between $0.35 \leqslant x \leqslant 0.75$. Synchrotron-based x-ray diffraction measurements have identified three film-to-substrate crystal orientations, with contributions from domains at 0°, ±18.43°, and ±30.96°. The relative contributions from these domains change dramatically with x. Surprisingly, the ±18.43° orientation dominates, particularly for high x, although it has the largest lattice mismatch to the underlying substrate. These results can only be explained by detailed modeling of the electrostatic forces between the ions at the film-substrate interface, and not with simplistic lattice mismatch arguments. Therefore, molecular dynamics simulations of the ionic heterogeneous interface structure of thin films of such large oxide systems have been performed in an attempt to explain the diffraction data. The simulations predict that, depending on x, an initial ultrathin layer of $SrNb_2O_6$ is favored, such that its Nb-O network forms the first ionic layer on the MgO(001) substrate. This provides the necessary template for the change in crystallographic orientation with x. Such layers were subsequently identified by further synchrotron-based x-ray-diffraction measurements. This information has important consequences for ferroelectric and electrooptic applications, on the optimal conditions required to grow thin films with large crystalline domains of the desired orientation.

DOI: 10.1103/PhysRevB.71.144114 PACS number(s): 68.55.Ac, 77.84.Dy, 81.15.Fg, 83.10.Rs

I. INTRODUCTION

The tetragonal metal oxide $Sr_xBa_{1-x}Nb_2O_6$ (SBN:x) is ferroelectric between $0.25 \leqslant x \leqslant 0.75$, and can exhibit an exceptionally large anisotropic electrooptic coefficient of the order of 1000 pm V^{-1}, some 40 times larger than that of the industry standard $LiNbO_3$.[1] As even modest voltages across thin films can produce large electric field strengths, the use of high-quality SBN:x thin films is especially attractive for optical switching, waveguiding, holography, surface acoustic wave devices, and information storage applications.

Figures 1(a) and 1(b) show the tetragonal structure of SBN:x, which has a unit cell containing 45 atoms.[2–7] High-quality films of such chemically and crystallographically complex structures can be grown using pulsed laser deposition (PLD),[8–12] mainly because of its ability to congruently transfer the material from the bulk to the growing surface. A second important property of PLD, and one that is often overlooked, is the rate of deposition. The average deposition rate is similar to that in MBE, of the order of 0.1 nm s^{-1}, and one can expect growth to be close to equilibrium, i.e., in a regime where kinetics play a secondary role. The *instantaneous* growth rate, i.e., that during the time the ablation plasma impinges on the substrate is, however, of the order of 10^3 nm s^{-1}. This induces a high degree of supersaturation above the growing surface, and a concomitant high density of nucleation sites. This is normally associated with the growth of films composed of many small crystallites, such as in rapid thermal deposition at low temperatures. However, the large time intervals between deposition events, typically of 0.1 s duration, and the enhanced surface diffusion resulting from transfer of kinetic energy of the impinging flux to the surface region, means that PLD is generally not kinetically hindered and is capable of producing films of the highest quality at reduced growth temperatures.[8]

The most common substrate on which to grow SBN:x has been MgO(001), due to its low refractive index at infrared and visible wavelengths. In addition, a second apriori reason for choosing MgO(001) as a suitable substrate is the small lattice mismatch δ between one unit cell of SBN:x and 3×3 unit cells of MgO. Between $x=0.35$ and $x=0.75$, this amounts to $\delta = +1.4\%$ to $+1.8\%$, whereby the positive sign indicates dilation in plane of the film. Despite this, such domains [Fig. 2(a)], with SBN:$x\langle 100\rangle$ parallel to MgO$\langle 100\rangle$, have until now not been observed.

Schwyn Thöny *et al.* found that although SBN:0.61 films grew with their c-axis perpendicular to the MgO(001) surface, the domains were twinned in-plane, with the SBN:$x\langle 100\rangle$ axes parallel to the MgO[310] and [130] equivalent axes [see Fig. 2(b)], i.e., at an angle of $\pm\arctan(1/3) = \pm 18.43°$ to the MgO[100] direction.[9] Based on heuristical arguments, they suggested that the large interface strain energy between SBN:0.61 and MgO at this angle could be offset by a lowering of the electrostatic energy and accommodated by strain relaxation after a number of monolayers.

Cuniot-Ponsard *et al.* discovered another set of in-plane twinned domains in SBN:0.67, which grew with its $\langle 100\rangle$ axes at an angle of ±31° to the MgO[100] axis.[11] Rouleau *et al.* found both twinned sets of domains in SBN:0.61, whereby they identified the larger angle of ±30.96° as $\pm\arctan(3/5)$ [Fig. 2(c)].

A recurring problem in comparing data from independent studies, such as outlined above, is that undocumented param-

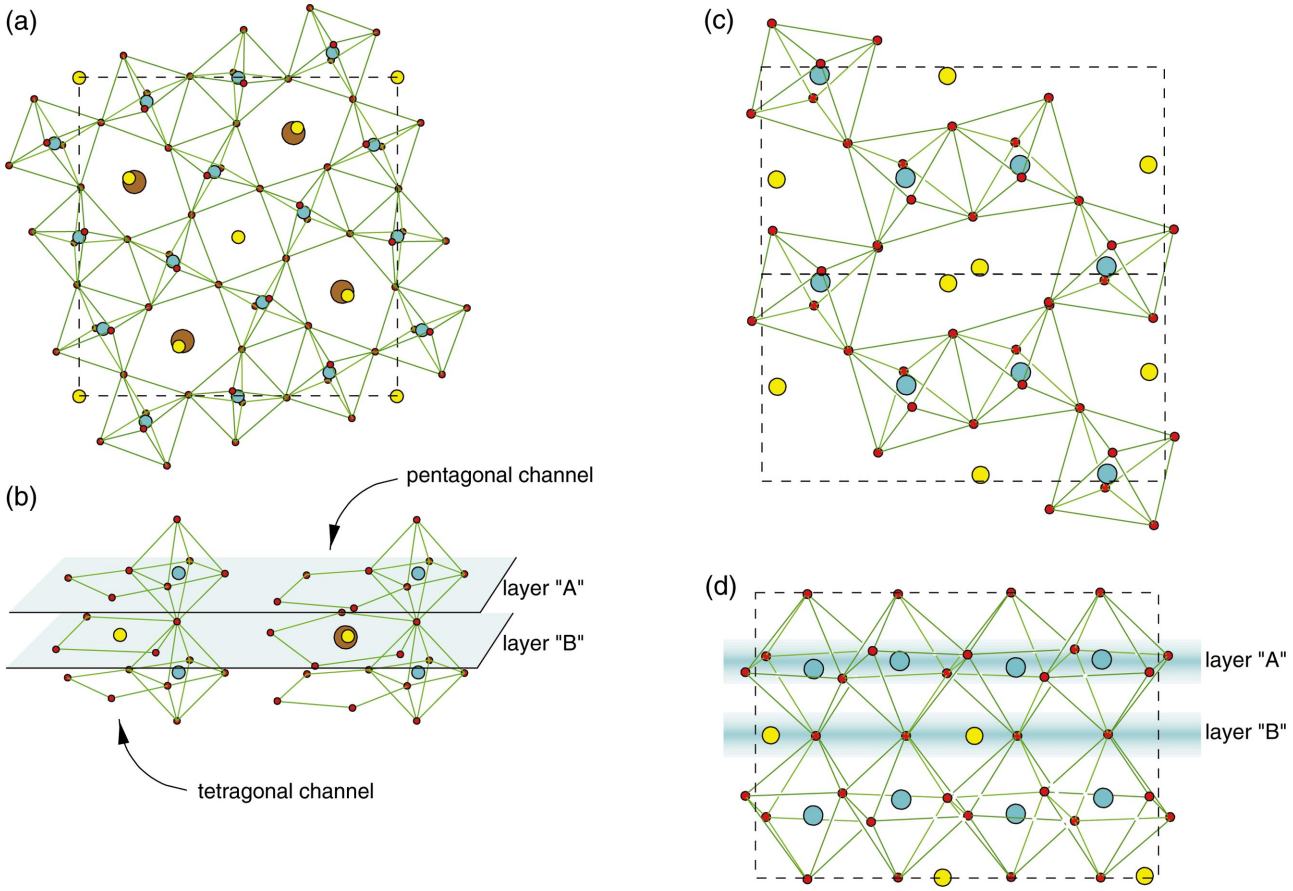

FIG. 1. (Color) The structures of SBN:x and $SrNb_2O_6$. (a) The projection of the unit cell of tetragonal SBN:x on the a-b plane. (b) Perspective schematic of the 12-fold coordinated (tetragonal) and the 15-fold coordinated (pentagonal) channels in SBN:x. (c) The projection of the $1\times2\times1$ cell of quasiorthorhombic $SrNb_2O_6$ (SNO) in the b-c plane and (d) on the a-c plane. In both structures, the planar region containing Nb ions is labeled layer "A," while that containing the Sr and Ba ions is layer "B." The dashed lines depict the unit cells. Color code: Mg: blue, O: red, Sr: yellow, Ba: brown, Nb: cyan.

eters in the film synthesis, such as materials quality, nucleation rates, and experimental geometry, can lead to seemingly contradictory results.[13] Therefore, we present a systematic study of the crystallographic nature of approximately 90-nm-thick SBN:x thin films with different compositions ($0.35\leqslant x\leqslant 0.75$), using synchrotron radiation. The films are grown on MgO(001) by a novel adaptation of PLD, which allows the choice of any film stoichiometry using just one ablation target.[14] Molecular dynamics (MD) simulations have provided a nucleation model that successfully describes the different crystallographic orientations of the SBN:x thin films with changing Sr content.

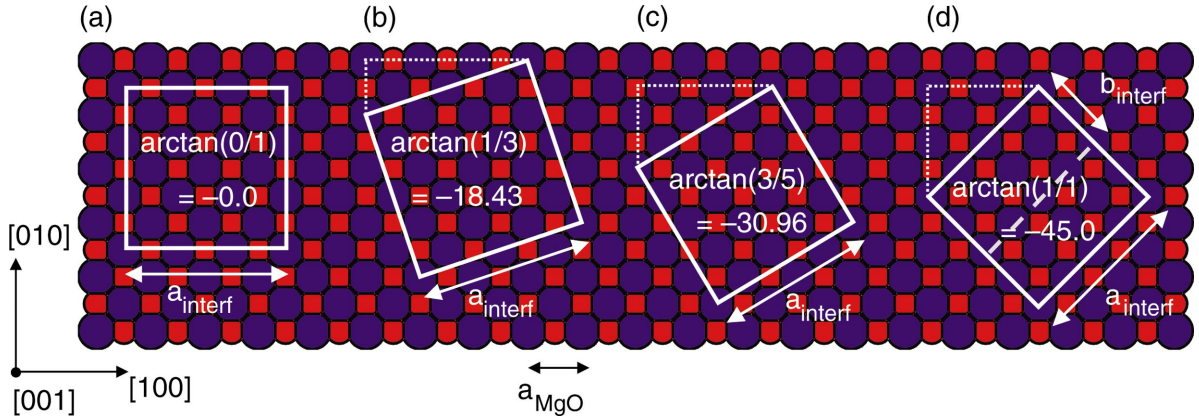

FIG. 2. (Color) Illustration of different film-to-substrate orientations. The three squares on the left depict tetragonal unit cells of SBN:x(001) on MgO(001), while the square on the right is the quasiorthogonal 2×1 cell of $SrNb_2O_6$(100) on MgO(001).

II. METHODS

A. Experimental

SBN:x films were grown by pulsed laser deposition (PLD) in conjunction with a synchronized N_2O gas pulse and an O_2 background gas[15] at a substrate temperature of 750 °C. Any desired Sr/Ba ratio could be achieved by using an ablation target rod consisting of a section of $SrNb_2O_6$ and another of $BaNb_2O_6$ and alternating between these in less time than that needed to grow one monolayer.[14,16] In contrast to growth of other SBN:x films reported in the literature, there was no need to postanneal the films in O_2, which we attribute to our use of the more oxidizing N_2O gas pulse.[17,18]

The film compositions were determined by Rutherford backscattering spectrometry (RBS) using 2 MeV ^{4}He projectiles, and also by heavy-ion RBS (HIRBS) using 15 MeV ^{29}Si projectiles, which allowed us to differentiate between Sr (atomic mass=87.6) and Nb (atomic mass=92.9). X-ray diffraction out-of-plane θ-2θ survey spectra were recorded using a Siemens D500 diffractometer with Cu $K\alpha$ radiation. All other x-ray data were collected at the surface diffraction station of the Materials Science beamline at the Swiss Light Source, Villigen, using 1 Å (12.398 keV) x radiation.

The quality of the in-plane crystallinity of the MgO substrates was checked by recording θ-2θ spectra and rocking curves of the in-plane MgO(200) reflection, which was found to have a width of less than 0.011° using 1 Å radiation. Using the Scherrer equation, this corresponds to domains with in-plane dimensions in excess of 450 nm, and negligible mosaicity. We could therefore conclude that low substrate quality can be excluded as an influence on the domain orientations and size of the thin films.

In-plane measurements of the SBN:x films were performed with the incident beam and detector axis set to 0.25° above the surface, i.e., marginally higher than the critical angle for SBN:x, which for $\lambda=1$ Å lies at $\approx$0.21° for the entire range of investigated stoichiometries. The in-plane domain orientations were established by setting the detector angle for the $2\theta_{(200)}\approx 9.2°$ reflection in the film plane, and rotating the sample about its surface normal by the angle ϕ.

B. Molecular dynamics simulations

The MD simulations are performed on model systems defined by simulation cells with three-dimensional periodic boundary conditions. The substrates and thin films are represented by slabs, i.e., systems periodically extended along the lattice vectors spanning the interface $\mathbf{a}_{\text{interf}}$ and with a finite size perpendicular to the interface, along the lattice vector **c**. The length of **c** is 8 nm.

All substrate models have two surface images, each in contact with a thin film slab (symmetric covering). The slab used for the MgO(001) substrate consists of nine layers and is $4a_{\text{MgO}}$ thick, where $4a_{\text{MgO}}$ is the lattice constant of MgO. The five innermost layers represent the bulk, and these ions are kept immobile in the simulations. The film-substrate interface regions are described by the mobile ions of the 2 sets of 2 outermost layers. Figures 2(a)–2(c) depict the in-plane dimensions of the substrate slabs directly in contact with SBN:x films for different orientations. The in-plane sizes of MgO(001) slabs coated with $SrNb_2O_6$(100) buffer layers and SBN:x(001) films are $a_{\text{interf}}=3\sqrt{8}a_{\text{MgO}}$ (±0.0°) and $a_{\text{interf}}=2\sqrt{10}a_{\text{MgO}}$ (±18.43°).

$SrNb_2O_6$ (SNO) buffer layers are always described with slabs that have the layer stacking "*ABAB*." SBN:x films on SNO(100) buffer layers are represented also by "*ABAB*" slabs, while the same films placed directly on MgO(001) by slabs that have the layer stacking 2× "*ABAB*." In all models, the two thin film types are separated by an approximately 2-nm-thick vacuum region along **c**, in order to electrostatically decouple them.

SBN:x slabs with two different compositions have been employed to examine the film ionic structure at the film-substrate interfaces at low and high Sr content, namely, with $x=0.3$ and $x=0.7$. Both compositions could be simulated easily and are close to the smallest and largest Sr-contents of the PLD-grown films.

To obtain energetically optimized ionic structures and interface energies, all model systems have been treated within a simulated melting and annealing approach. The melting procedure consists of MD simulations for 100-150 ps at 0 K, and 50 ps at 50, 200, 400, and 600 K. After, the systems are quenched with simulations for 50 ps at 600 and 300 K and finally for 100-150 ps at 0 K. A time step of 3 fs has been used in the MD simulations. The calculations were performed with the GULP code.[19] The interionic potentials used are based on the Born model of ionic solids, in which ions are described as rigid spheres and interact via long-range Coulombic interactions and short-range, parametrized interactions. The potential parameters are taken from Woodley *et al.*[20]

III. RESULTS AND DISCUSSION

Representative x-ray diffraction (XRD) spectra of our films are given in Fig. 3. Figure 3(a) shows the out-of-plane θ-2θ spectrum, demonstrating c-axis growth, and in-plane data are shown in Fig. 3(b). In addition to the two known in-plane orientations at ±18.43° and ±30.96°, the as yet unreported domain with the SBN[100] axis parallel to the MgO[100] axis (0.0° orientation) was discovered. The relative contributions of each domain orientation, $f_{\pm\phi}$, could be calculated by integrating the peak signals. Normalizing to unity, we obtain

$$f_{\pm\phi}=\frac{\int_{\text{peak}} I_{+\phi}d\phi+\int_{\text{peak}} I_{-\phi}d\phi}{\sum\int_{\text{peak}} I_{\phi}d\phi}, \tag{1}$$

where the summation in the denominator is over the five domains found at 0, ±18.43, and ±30.96, and the second term in the numerator is ignored for $\phi=0°$, as the fourfold symmetry of the MgO(001) surface means that the 0° domain is not twinned. The results are summarized in Fig. 3(c). At low x, we observe a mixed orientational composition containing all three domain types. The composition changes with in-

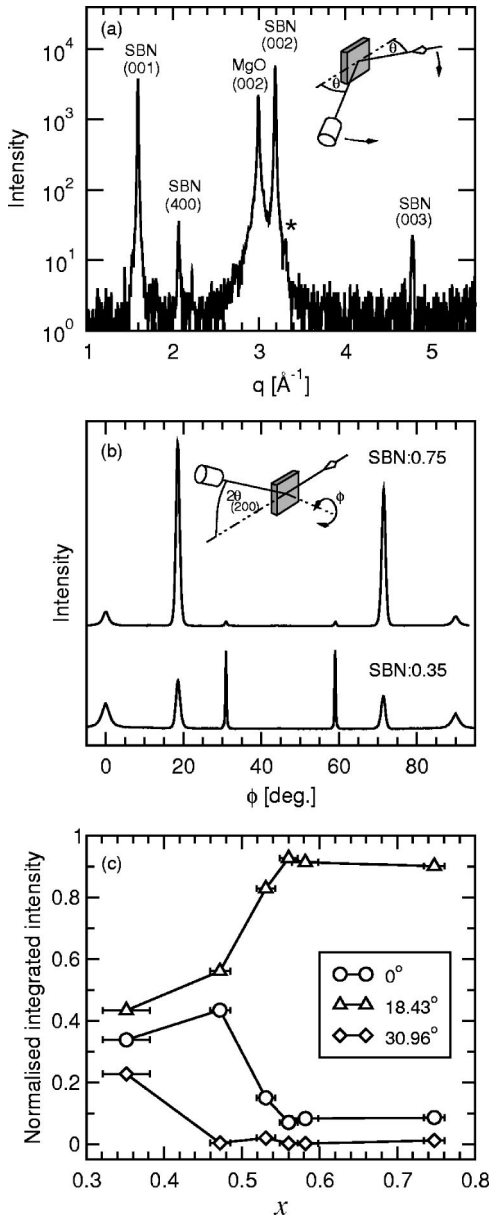

FIG. 3. Crystallographic data of SBN:x. (a) θ-2θ scan of a typical SBN:x film grown on MgO(001) using Cu $K\alpha$ radiation, as a function of $q=4\pi \sin\theta/\lambda$. (b) In-plane scans showing the different domain orientations for SBN:0.35 and SBN:0.75, using synchrotron radiation at 1 Å. The detector was placed at a fixed in-plane angle of $2\theta_{(200)}$ for the (200) reflection of SBN:x. The sample was rotated by ϕ around its normal axis. (c) The relative contributions of each domain type as a function of x, acquired by integrating the peaks in (b), using Eq. (1).

creasing x, to one that is dominated by the ±18.43° orientation for $x \geqslant 0.55$, despite the fact that it is this orientation that has the largest lattice mismatch to the underlying substrate.

The c- and a-axis lattice constants and crystallite sizes were determined by θ-2θ-scans and rocking curves out-of-plane and in-plane, respectively. The out-of-plane crystallite size, determined by the Scherrer equation, is of the order of the film thickness of 90 nm, indicative of columnar film growth. The thin film SBN:x in-plane lattice constants deviate by no more than 0.2% from the bulk literature values.

TABLE I. Interface lattice parameters of SBN:x, $0.35 \leqslant x \leqslant 0.75$, and $SrNb_2O_6$ (SNO) on MgO(001) for different film-to-substrate orientations ω (in degrees).

	SBN:x, $0.35 \leqslant x \leqslant 0.75$			SNO
ω	0.00	±18.43	±30.96	±45.00
δ [a]	$1.26 \rightarrow 1.70$	$6.52 \rightarrow 6.96$	$-1.60 \rightarrow -1.16$	7.3
a_{interf} [b]	3	$\sqrt{10}$	$\sqrt{8.5}$	$2\sqrt{2}$

[a]Lattice mismatch (in %).
[b]Characteristic length of the interface unit cell in units of the MgO lattice constant a_{MgO} (see Fig. 2).

The fact that the consistently dominant 18.43° orientation is the one with the largest lattice mismatch suggests that the electrostatic forces between the highly charged cations and anions at the film-substrate interface play a critical role. Hence we can assume that the strain between the film and substrate must be relaxed either by crystallographic faults or by a transitional (buffer) layer of another structure.

The key questions to understand the change of the domain orientation with x are as follows (i) What is the SBN:x interface layer, and does it begin with a Nb-O or Sr-O/Ba-O

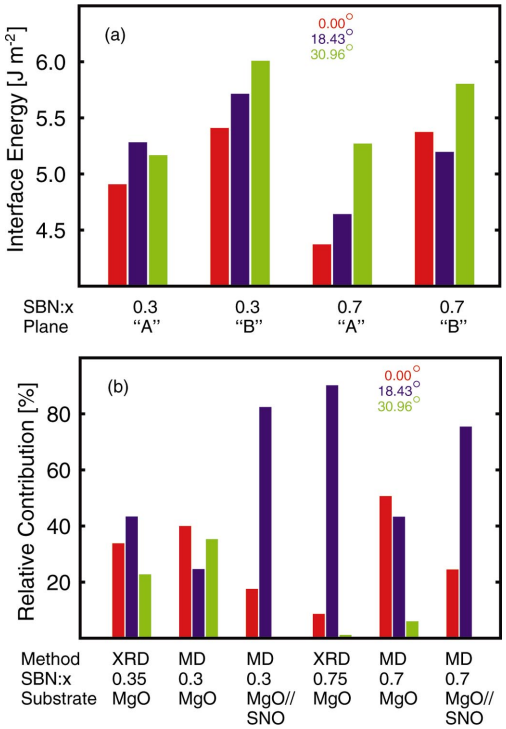

FIG. 4. (Color) Results of the MD simulations. (a) Interface energies calculated with Eq. (2) for the model systems where SBN:x(001) films are directly in contact with MgO(001), either with layer "A" or "B." The smaller the interface energy is, the stronger is the film-substrate interaction. (b) Comparison of the experimental relative orientational distributions $f_{\pm\phi}$ with those predicted by the MD simulations p_i at low and high Sr-content x, both with and without SNO buffer layers. "MgO//SNO" means a MgO substrate coated with an SNO buffer layer. In all calculations in (b), the first SBN:x interface atomic layer is the Nb-O "A" layer.

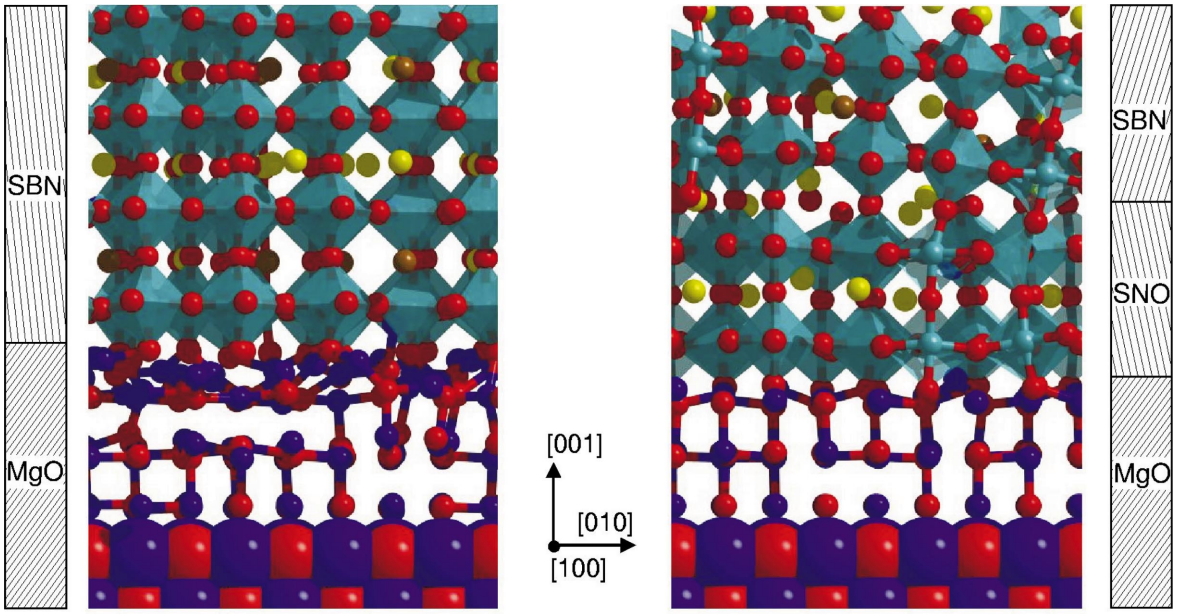

FIG. 5. (Color) Calculated ionic structures of substrate-thin film interfaces. Left: SBN:0.7(001) on MgO(001). Right: SBN:0.7(001) on MgO(001) coated with a SNO(100) buffer layer. The buffer layer has an in-plane orientation with respect to MgO of ±45°, whereas SBN:x has in both structures an in-plane orientation with respect to MgO of ±18.43°. The panels on the outer left and outer right depict the sequence of MgO, SBN, and SNO. The large balls represent the MgO ions of the bulk while the small balls the ions of the interface layers. The polygons emphasize NbO_6 octahedra, while the sticks depict ionic distances smaller than the sum of the appropriate ionic radii. The color code is as in Fig. 1.

ionic layer ("A" and "B" in Fig. 1, respectively)? (ii) Why is the orientation with the largest lattice mismatch always the preferred orientation? (iii) Why do the 0° and ±30.96° orientations almost disappear for $x > 0.55$?

To answer the first key question, we have performed MD simulations on model systems where SBN:0.3 and SBN:0.7 films are in direct contact with MgO(001). The MD simulations yield ionic configurations optimized with respect to the potential energy of the film-substrate system, $E_{\text{TF-substr}}$. Note that the potential energy includes only the long-range Coulombic interactions and short-range interactions between the ions. For instance, entropy contributions were not taken into account. To quantify the strength of the film-substrate interactions of the three relevant film-to-substrate orientations (0.0°, 18.43° and 30.96°), we have introduced an interface energy E_{interf} which is defined as

$$E_{\text{interf}} = \frac{E_{\text{TF-substr}} - n_{\text{MgO}} E_{\text{MgO}} - n_{\text{SBN:}x} E_{\text{SBN:}x}}{a_{\text{interf}}^2}. \qquad (2)$$

In Eq. (2), E_{MgO} and $E_{\text{SBN:}x}$ are the potential energies per formula unit of the optimized bulk structures of MgO and SBN:x, respectively. The terms n_{MgO} and $n_{\text{SBN:}x}$ are the corresponding number of formula units used to construct the model systems. The characteristic lengths of the interface unit cells a_{interf} are summarized in Table I.

The interface energies are always positive because we compare potential energies of systems with and without surfaces, i.e., slabs and bulk systems, respectively. Therefore, the criterion is the smaller E_{interf} is, the stronger is the film-substrate interaction. Figure 4(a) depicts the derived interface energies.

For all orientations, the electrostatic energy is minimized if the first ionic layer above MgO is the Nb-O network, i.e., layer "A" in Fig. 1(b), as first predicted by Schwyn Thöny *et al.*[9] The very strong Coulomb attraction between the highly positively charged Nb cations and the oxygen anions is the decisive factor.

To obtain quantitative answers to the second and third key questions, the results of the MD simulations must be directly comparable with the experimentally determined relative contribution of each domain type $f_{\pm\phi}$. Therefore, the calculated interface energies of each domain orientation have been converted to the relative contributions p_i using the partition function

$$p_i = \frac{g_i e^{-E_{\text{interf},i}/nk_BT}}{\sum_j g_j e^{-E_{\text{interf},j}/nk_BT}}. \qquad (3)$$

In Eq. (3), k_B is the Boltzmann constant, T is the absolute temperature, and g_i is the degeneracy of the ith domain, equal to unity for the 0° domain and 2 for the ±18.43° and ±30.96° domains. The argument of the exponent contains $n = 2.254 \times 10^{19}$ m^{-2}, the areal bond density of the MgO surface, which is required to convert E_{interf} to a bond energy. The temperature was taken to be the growth temperature of 1023 K, whereby it has been assumed that the rapid cooling after film growth kinetically precludes any change in the orientational distribution. The results are summarized in Fig. 4(b).

First, let us compare the experimental and calculated orientational distributions for low x [left-hand side of Fig. 4(b)]. The MD simulations on the models in which SBN:x grows directly on MgO yielded relative contributions in fair agreement with experiment - the calculated contributions of the 0° and ±30.96° orientations are somewhat larger than the experimental values, while that of the ±18.43° orientation is slightly smaller than found experimentally. Therefore, the experimentally determined orientational distribution at low x can be explained with SBN:x(001) films with their layer "A" directly grown on MgO(001).

In the case of SBN:0.7, however, the calculations for film growth directly on MgO(001) yielded relative contributions of the 0° and ±18.43° orientations that were much too large and too small, respectively, compared with the XRD results. This model therefore predicts that, for high Sr content, the severe lattice mismatch of the ±18.43° domains is the dominant factor and affects their formation negatively. Hence, ionic configurations in which SBN:x is directly in contact with MgO cannot explain why the ±18.43° orientation is always preferred and why the 0° and ±30.96° orientations almost disappear for $x>0.55$.

Some studies have hinted that, in thin film growth of SBN:x, $SrNb_2O_6$ (SNO) might segregate out at the film-substrate interface, depending on x, and also on the growth conditions.[11,21] This stimulated us to consider a second model, in which a thin SNO buffer layer is introduced at the film-substrate interface, with its [010] axis parallel to the two equivalent MgO[110] and $[\bar{1}10]$ axes (i.e., an SNO in-plane orientation of ±45°, see Fig. 2). In order to calculate the interface energies E_{interf} for the second model, an additional term $-n_{\text{SNO}}E_{\text{SNO}}$ is added to the numerator of Eq. (2). The terms E_{SNO} and n_{SNO} are the potential energy per formula unit of the optimized bulk structure of SNO and the corresponding number of formula units to construct the SNO buffer layer, respectively. The first ionic layer of SNO(100) above MgO(001) is also the Nb-O network, i.e., layer "A" in Fig. 1(d), as predicted by prior MD simulations.

The relative contributions p_i for high Sr content, derived from the MD simulations of the second model, are in excellent agreement with the experimental relative contributions for $x>0.55$ [right-hand side of Fig. 4(b)]. This result is at first sight surprising, considering the large lattice mismatch between SNO and MgO, comparable to that of the ±18.43° SBN:x domains (see Table I). However, SNO is a more flexible structure [see Fig. 1(c)], with the oxygen octahedra connected to one another not just at their vertices, as in SBN:x, but also along their edges, making it more easily distorted.

Figure 5 shows energetically optimized ionic structures of the first model, involving only MgO and SBN:0.7, and the second model, which includes an SNO buffer layer, both at a film-to-MgO substrate orientation of ±18.43°. One can immediately identify the higher degree of order of the magnesium and oxygen ions at the interfacial region when SNO is included, compared to the semi-amorphous interface when SBN:0.7 is in direct contact with the MgO surface. The higher order is the reason for a stronger electrostatic attraction between film and the substrate and, hence, the large

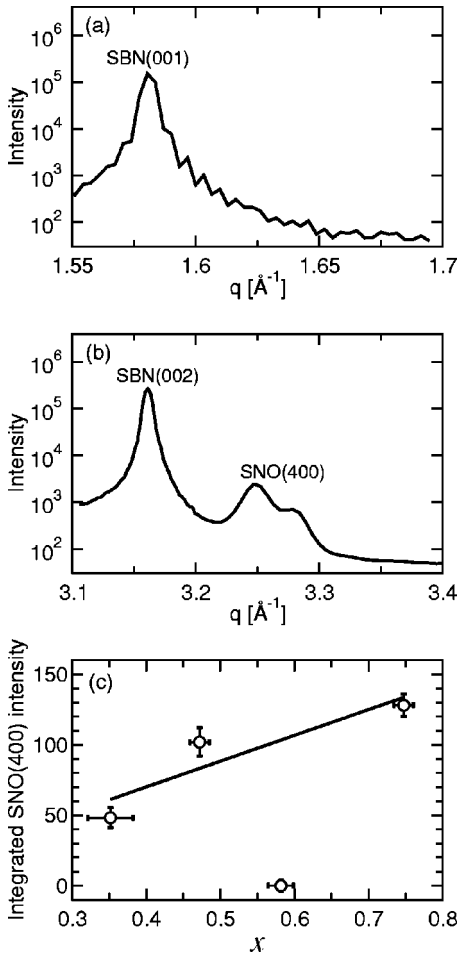

FIG. 6. Evidence of a $SrNb_2O_6$ buffer layer. (a) and (b): θ-2θ spectra of SBN:0.47 on MgO as a function of $q=4\pi\sin\theta/\lambda$. The SNO(200) peak at $q=1.63$ Å^{-1} is missing, because, when distorted into a tetragonal unit cell, it becomes a forbidden reflection. The (400) reflection at $q=3.26$ Å^{-1}, however, is clearly visible. (c) The integrated SNO(400) peak intensity as a function of the Sr-content x. Ignoring the anomalous data point at $x=0.58$, the SNO signal increases monotonically with x. The straight line is a guide to the eye.

relative contribution of $p_i\approx 80\%$ [see Fig. 4(b)]. Hence, on the one hand, the SNO buffer layer accommodates growth of the ±18.43° in-plane orientation of SBN:x, while on the other, the buffer layer adversely affects the formation of SBN:x domains with orientations of 0° or ±30.96°. It seems reasonable that the relative contributions of the orientations will also depend on the size of the characteristic repetition length describing the interfaces a_{interf}. Interfacial unit net areas a_{interf}^2 which are large must accommodate concomitantly large numbers of bond sites that may or may not be favorable. Indeed, for the ±30.96° orientation, $a_{\text{interf}}=2\sqrt{34}a_{\text{MgO}}$ ($\approx$49 Å) and the unit net contains some 544 interfacial ionic bonds. The probability is negligible that these bonds will repetitively form in a regular manner with a periodicity of a_{interf} which explains why the growth of SBN:x with an orientation of ±30.96° on an SNO buffer layer is suppressed.

The good agreement between the MD simulations including a buffer layer of SNO and our experimental data led us to

more closely inspect the laboratory-based spectra. They indicated the possible presence of a very weak SNO(400) peak at the expected position, labeled with an asterisk in Fig. 3(a).

We therefore reinvestigated the films using synchrotron-based x-ray diffraction. Depending on x, a clear, if weak, signal was found in the θ-2θ spectra at the expected q value for SNO(400), although no SNO(200) peak was found, despite the fact that the ratio of their intensities in powder diffraction spectra should be 0.44 [Figs. 6(a) and 6(b)]. In the MD simulations, however, it turns out that the SNO is distorted from a quasiorthorhombic cell to a tetragonal cell, in which the octahedra become coaxial parallel to the b axis and the atoms within layers "A" and "B" become exactly coplanar. The SNO(200)/SNO(400) intensity ratio in this case was calculated to be only 2×10^{-3}, hence the SNO(200) signal is suppressed. The observed SNO(400) signal increases on average with x [Fig. 6(c)].

Why should SNO be promoted? Oral and Mecartney have suggested that fast nucleation processes, such as occurs in PLD,[8] will induce crystallization of the SNO phase.[21] A second source of nucleation centers may be the microscopic morphology of the MgO surface, which is known to be rough on the Å scale. Rouleau *et al.* could suppress the ±30.96° domains by using MgO substrates with a 2° miscut. It was suggested that the fourfold symmetry of the substrate was thereby reduced to twofold symmetry, which suppressed these domains.[12] A 2° substrate miscut means, however, that the terraces have an average extent of some 12 nm, which is over 10 times the SBN:x unit cell in-plane lattice constant. On the other hand, the higher density of terrace edges in the miscut substrate will increase the density of nucleation and crystallization sites for SNO. The MD simulations show that the SNO buffer layer, with an orientation of ±45° with respect to the MgO substrate, strongly adversely affects the growth of the ±30.96° domains. This could be the reason for their complete suppression when using miscut MgO substrates.

IV. CONCLUSIONS

We have used a novel adaptation of PLD to grow $Sr_xBa_{1-x}Nb_2O_6$ thin films with their (001) plane on MgO(001) substrates. For Sr content from $x=0.35$ to 0.55, three film-to-substrate in-plane orientations with contributions of $\pm18.43°>0°>\pm30.96°$ could be identified. MD simulations could model this orientational distribution to ionic configurations in which SBN:x grows directly on MgO. However, for stoichiometries of $0.55<x\leqslant0.75$, this model completely fails to predict the experimentally observed fact that the ±18.43° orientation dominates while the contributions of the other two orientations are effectively suppressed. However, for high Sr contents, MD simulations also predicted the nucleation of SNO in a thin interfacial buffer region, which promotes the growth of an otherwise highly mismatched but electrostatically favored SBN:x crystal orientation of ±18.43°. These predictions were subsequently supported by further synchrotron-based x-ray diffraction measurements. The MD simulations predict also that SBN:x(001) as well as SNO(100) grow on MgO(001) such that its Nb-O network forms the first ionic layer on the substrate. The dependence of the nucleation of SNO on the surface on other factors, such as the roughness and miscut of the substrate, should be further investigated.

ACKNOWLEDGMENTS

Support of this work by the Schweizerischer Nationalfonds zur Förderung der wissenschaftlichen Forschung is gratefully acknowledged. The authors would like to thank M. Lange and D. Meister for their assistance in construction of the deposition chamber, A. Al-Adwan and D. Maden for their help in software and interface development, and M. Döbeli for his assistance with the RBS measurements. One of the authors (R.W.) is especially grateful for the computer time and the support provided by the computing division of the Paul Scherrer Institute.

*Email address: philip.willmott@psi.ch

[1] O. Eknoyan, H. F. Taylor, J. M. Marx, Z. Tang, and R. R. Neurgaonkar, Ferroelectrics **205**, 147 (1998).
[2] P. B. Jamieson, S. C. Abrahams, and J. L. Bernstein, J. Comput. Phys. **48**, 5048 (1968).
[3] J. R. Carruthers and M. Grasso, J. Electrochem. Soc. **117**, 1426 (1970).
[4] T. S. Chernaya, B. A. Maksimov, I. V. Verin, L. I. Ivleva, and V. I. Simonov, Crystallogr. Rep. **42**, 375 (1997).
[5] T. S. Chernaya, B. A. Maksimov, T. R. Volk, L. Ivleva, and V. I. Simonov, Phys. Solid State **42**, 1716 (2000).
[6] D. Schaniel, J. Schefer, V. Petricek, M. Imlau, R. Pankrath, T. Granzow, and T. Woike, Appl. Phys. A: Mater. Sci. Process. **74**, S963 (2002).
[7] T. Woike, V. Petricek, M. Dusek, N. K. Hansen, P. Fertey, C. Lecomte, A. Arakcheeva, G. Chapuis, M. Imlau, and R. Pankrath, Acta Crystallogr., Sect. B: Struct. Sci. **59**, 28 (2003).
[8] P. R. Willmott, Prog. Surf. Sci. **76**, 163 (2004).
[9] S. Schwyn Thöny, K. E. Youden, J. S. Harris, Jr., and L. Hesselink, Appl. Phys. Lett. **65**, 2018 (1994).
[10] K. Tanaka, O. Nakagawara, M. Nakano, T. Shimuta, H. Tabata, and T. Kawai, Jpn. J. Appl. Phys., Part 1 **37**, 6142 (1998).
[11] M. Cuniot-Ponsard, J. M. Desvignes, B. Ea-Kim, and E. Leroy, J. Appl. Phys. **93**, 1718 (2003).
[12] C. M. Rouleau, G. E. Jellison, Jr., and D. B. Beach, Appl. Phys. Lett. **82**, 2990 (2003).
[13] G. K. Hubler and J. A. Sprague, Surf. Coat. Technol. **81**, 29 (1996).
[14] P. R. Willmott, R. Herger, and C. M. Schlepütz, Thin Solid Films **453-454**, 436 (2003).
[15] P. R. Willmott and J. R. Huber, Rev. Mod. Phys. **72**, 315 (2000).
[16] P. R. Willmott, R. Herger, M. C. Falub, L. Patthey, M. Döbeli, C. V. Falub, M. Shi, and M. Schneider, Appl. Phys. A: Mater. Sci. Process. **79**, 1199 (2003).

[17] A. Gupta and B. W. Hussey, Appl. Phys. Lett. **58**, 1211 (1991).
[18] P. Lecoeur, A. Gupta, P. R. Duncombe, G. Q. Gong, and G. Xiao, J. Appl. Phys. **80**, 513 (1996).
[19] J. D. Gale and A. L. Rohl, Mol. Simul. **29**, 291 (2003).
[20] S. M. Woodley, P. D. Battle, J. D. Gale, and C. R. A. Catlow, Phys. Chem. Chem. Phys. **1**, 2535 (1999).
[21] A. Y. Oral and M. L. Mecartney, J. Mater. Res. **15**, 1417 (2000).